Theranostic Probe Based on Lanthanide-Doped Nanoparticles for Simultaneous In Vivo Dual-Modal Imaging and Photodynamic Therapy

ARTICLE *in* ADVANCED MATERIALS · NOVEMBER 2012

Impact Factor: 17.49 · DOI: 10.1002/adma.201202433 · Source: PubMed

18 AUTHORS, INCLUDING:

Hyung Min Kim
Kookmin University
37 PUBLICATIONS **958** CITATIONS
SEE PROFILE

Wooram Park
Northwestern Feinberg School of Medicine
30 PUBLICATIONS **538** CITATIONS
SEE PROFILE

Daishun Ling
Zhejiang University
26 PUBLICATIONS **406** CITATIONS
SEE PROFILE

Woo Kyung Moon
Seoul National University Bundang Hospital
334 PUBLICATIONS **5,865** CITATIONS
SEE PROFILE

Theranostic Probe Based on Lanthanide-Doped Nanoparticles for Simultaneous In Vivo Dual-Modal Imaging and Photodynamic Therapy

Yong Il Park, Hyung Min Kim, Jeong Hyun Kim, Kyung Chul Moon, Byeongjun Yoo, Kang Taek Lee, Nohyun Lee, Yoonseok Choi, Wooram Park, Daishun Ling, Kun Na, Woo Kyung Moon, Seung Hong Choi, Hong Seok Park, Soo-Young Yoon, Yung Doug Suh, Sung Ho Lee,* and Taeghwan Hyeon**

Typical molecular imaging methods, such as fluorescence imaging and magnetic resonance imaging (MRI), have different sensitivities, spatial resolutions, and imaging depths.[1,2] In vivo fluorescence imaging provides high sensitivity and temporal resolution; however, penetration of visible light in living tissues is not efficient and spatial resolution is limited. MRI can produce non-invasive images with functional information and high spatial resolution anatomic details based on soft-tissue contrast; however, its sensitivity is relatively lower than other whole body imaging methods such as positron emission tomography (PET). Therefore, various multimodal imaging probes combining different imaging modalities have been developed for more accurate imaging and diagnosis.[3] For example, nanoparticles combining fluorescence imaging modality and MRI modality can offer the advantages of fluorescence imaging, i.e., high sensitivity, along with the high spatial resolution anatomic imaging capability of MRI.[4]

Recently, anti-Stokes fluorophores, which emit shorter wavelength light than excitation energy, have been proposed as next-generation luminescent probes.[5] Among various anti-Stokes processes, the upconversion process[6] is more efficient than second-harmonic generation (SHG)[7] or two-photon absorption (TPA),[8] because the upconversion process relies on multiple metastable energy levels. In the last decade, several studies on the synthesis and biomedical applications of upconverting nanoparticles (UCNPs) have been reported.[9] Because a near-infrared (NIR) continuous-wave (CW) diode laser can be used as an excitation source, it can increase the penetration depth and suppress autofluorescence in biological samples.[10] Moreover, UCNPs have high photostability and exhibit neither photoblinking nor photobleaching.[11] In addition, they are less toxic than quantum dots composed of toxic heavy metal ions such as Cd^{2+}.[12] Recently, $NaGdF_4$-based UCNPs have been developed as multimodal imaging probes,[11a,13] and applied to animal studies.[14] Gd ions incorporated in the host matrix could enhance the contrast in T1 MRI.[11a,13a]

Furthermore, the energy conversion process of UCNPs can be exploited for therapeutic applications such as photodynamic therapy (PDT). Administered PDT drugs (photosensitizers) are activated by light; they generate cytotoxic reactive oxygen species (ROS) from surrounding water molecules and induce cell death. PDT has long been used as an effective and non-invasive treatment for premalignant and malignant tumors.[15] Most photosensitizers for PDT are activated by visible light, which

Prof. T. Hyeon, Dr. Y. I. Park, Dr. J. H. Kim, B. Yoo, Dr. N. Lee, D. Ling
World Class University (WCU) Program of Chemical Convergence for Energy & Environment (C2E2),
Institute of Chemical Processes
School of Chemical and Biological Engineering
Seoul National University
Seoul 151-744, South Korea
E-mail: thyeon@snu.ac.kr
Dr. H. M. Kim, Dr. K. T. Lee, Dr. Y. D. Suh
Laboratory for Advanced Molecular Probing (LAMP)
Research Center for Convergence Nanotechnology
Korea Research Institute of Chemical Technology (KRICT)
Daejeon 305-600, South Korea
Prof. S.-Y. Yoon, K. C. Moon
Department of Laboratory Medicine
Korea University Ansan Hospital
College of Medicine, Korea University
Ansan 425-707, South Korea
E-mail: labmd@korea.ac.kr

DOI: 10.1002/adma.201202433

Prof. S. H. Choi, Prof. W. K. Moon, Y. Choi
Diagnostic Radiology
Seoul National University Hospital and the Institute of Radiation Medicine, Medical Research Center
Seoul National University
Seoul 110-744, South Korea
Prof. K. Na, W. Park
Department of Biotechnology
The Catholic University of Korea
Bucheon-si, Gyeonggi-do 420-743, South Korea
Prof. H. S. Park
Department of Urology
Korea University Guro Hospital
College of Medicine, Korea University
Seoul 152-703, South Korea
Prof. S. H. Lee
Department of Thoracic and Cardiovascular Surgery
Korea University Anam Hospital
College of Medicine, Korea University
Seoul 136-705, South Korea
E-mail: sholeemd@korea.ac.kr

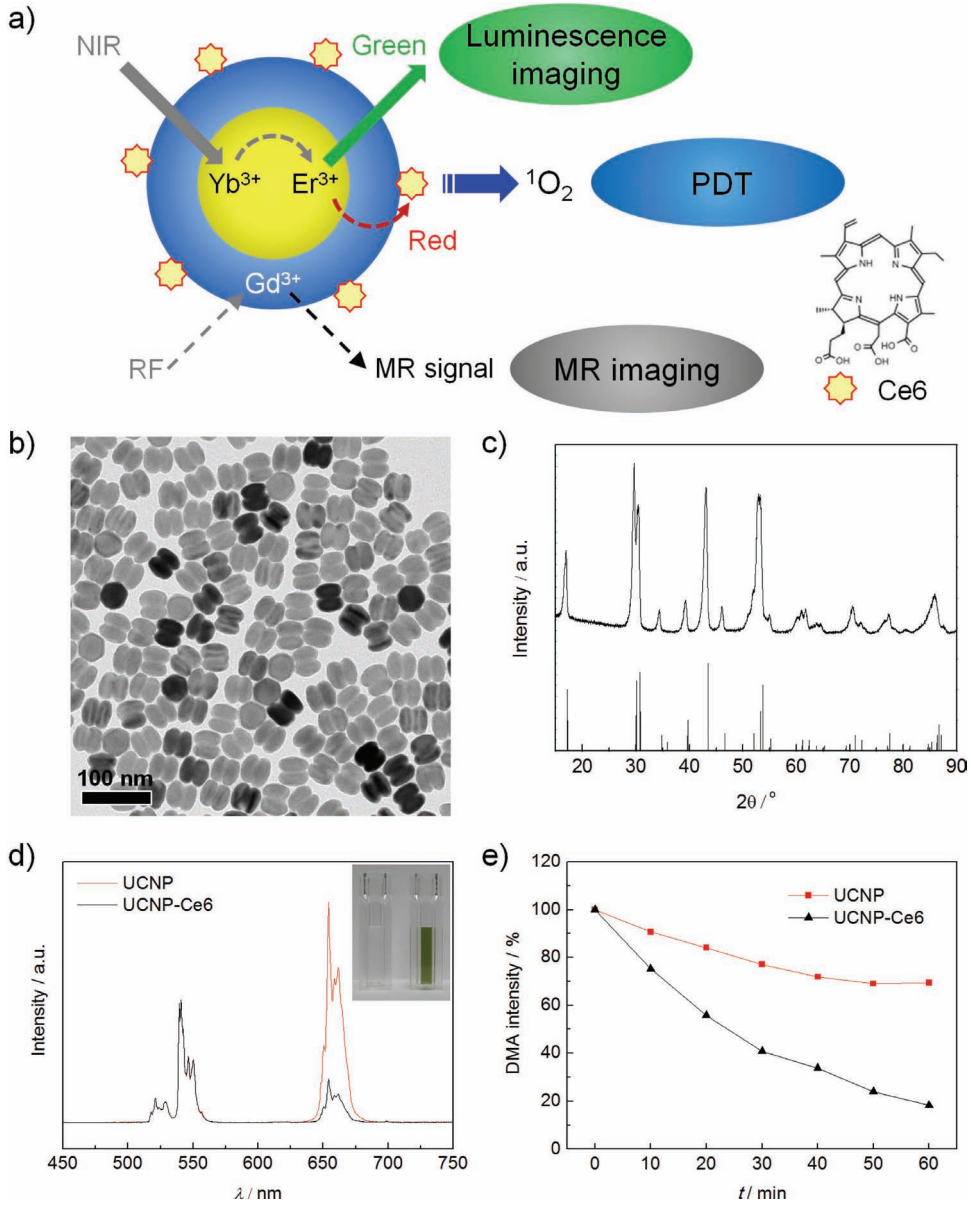

Figure 1. a) Schematic illustration of dual-modal imaging and PDT using UCNP–Ce6. b) Transmission electron microscopy (TEM) image of core–shell UCNPs. c) XRD pattern of core–shell UCNPs. Bottom line pattern is that of hexagonal phase $NaYF_4$ (JCPDS 16-0334). d) Emission spectra of UCNPs and UCNP–Ce6 under 980 nm excitation. Inset is the photograph of UCNPs (colorless) and UCNP–Ce6 solutions (green). e) Change of DMA fluorescence due to generation of singlet oxygen from UCNPs and UCNP–Ce6 under 980 nm irradiation.

has limited penetration depth in living tissue. When UCNPs are combined with PDT drugs, the NIR-to-visible upconversion capability of UCNPs can be used to excite photosensitizers through energy transfer, thereby activating drugs located deep in the tissue. The therapeutic effects of UCNP-PDT drug combinations have been reported in cellular-level and animal studies.[16] However, there have been no previous reports on the systemic administration of UCNP-based PDT agents. Herein, we report on dual-modal in vivo tumor imaging and PDT treatment using UCNPs combined with photosensitizers (**Figure 1**a and Scheme S1 in the Supporting Information). Hexagonal phase $NaYF_4$:Yb,Er/$NaGdF_4$ core–shell UCNPs were used for upconversion luminescence imaging and MRI. Owing to the enhanced permeability and retention (EPR) effect, intravenously injected UCNPs were accumulated at the tumors. For inducing a therapeutic effect, a photosensitizer, chlorin e6 (Ce6), was incorporated in the UCNPs. The resulting UCNPs conjugated with Ce6 (UCNP–Ce6) were systemically administered, and could be used as contrast agents to clearly visualize tumors. We also demonstrated the therapeutic effect of UCNP–Ce6 in vivo under 980 nm irradiation.

For highly efficient upconversion luminescence, hexagonal phase UCNPs with a core–shell structure were synthesized using the previously reported method[9c,17] with some modifications.

As-synthesized $NaYF_4$:Yb,Er nanoparticles had a rod shape and a dimension of 33 nm (diameter) × 40 nm (length) (Figure S1, Supporting Information). In order to enhance upconversion luminescence[9f] and T1 MRI contrast,[11a] a $NaGdF_4$ shell was added to the $NaYF_4$:Yb,Er core nanoparticles, obtaining $NaYF_4$:Yb,Er/$NaGdF_4$ core–shell nanoparticles with a dimension of 42 nm (diameter) × 42 nm (length) (Figure 1b and Figure S2 in the Supporting Information). Elemental analysis using inductively coupled plasma atomic emission spectroscopy (ICP-AES) revealed the composition of the as-synthesized UCNPs (Table S1, Supporting Information). X-ray diffraction (XRD) patterns (Figure 1c) confirmed that the as-synthesized core–shell UCNPs had a hexagonal phase crystal structure (JCPDS 16-0334). The emission spectrum of the as-synthesized UCNPs (Figure 1d) displayed characteristic green and red emission bands that correspond to the transitions from the emitting energy levels of Er ions. The two green bands are attributed to Er transitions from $^2H_{11/2}$ to $^4I_{15/2}$ (520–540 nm) and $^4S_{3/2}$ to $^4I_{15/2}$ (540–560 nm), whereas the red emission band is attributed to the Er transition from $^4F_{9/2}$ to $^4I_{15/2}$ (640–680 nm).

Water-dispersible and amine-functionalized UCNPs encapsulated by poly(ethylene glycol) (PEG)-phospholipids were prepared by the method described previously with some modifications.[11a] For the therapeutic applications of UCNPs as PDT agents, UCNPs were combined with a photosensitizer, Ce6. Most photosensitizers are activated by visible light, and thus the shallow penetration depth of incident light has limited their wide applications.[15,18] If the absorption of a PDT drug can be extended to the NIR range, the activation light can reach deeper into the lesion, and thus significantly improve the efficacy. The red emission from UCNPs is well matched with the absorption peak of Ce6 (Figure S3, Supporting Information), and the energy transfer from UCNP to Ce6 enables indirect activation of the photosensitizer by NIR light.[16] In order to maximize the loading of Ce6, physical adsorption of Ce6 onto the particle surface and chemical conjugation between the UCNPs and Ce6 were combined. Owing to the hydrophobic property and planar structure of chlorin, Ce6 could be readily entrapped in hydrophobic phospholipid layers surrounding the UCNPs. In addition, the 1-ethyl-3-(3-dimethylaminopropyl) carbodiimide hydrochloride (EDC) coupling reaction between the amine-functionalized UCNPs (>10^3 amine group per particle, Figure S4, Supporting Information) and the carboxy group of Ce6 was employed to form an amide bond. After purification by column chromatography and centrifugation, the color of the resulting UCNP–Ce6 was green, which is the characteristic color of Ce6; this indicated the successful conjugation of UCNPs with Ce6 (Figure 1d, inset). The amount of Ce6 calculated from the UV–vis absorption spectra was found to be >10^3 Ce6 per particle. As the amount of added Ce6 increased, the absorption peak at 660 nm also increased (Figure S5, Supporting Information). The absorption measurement verified the additional increase in Ce6 loading by the EDC reaction. The loading of Ce6 on the particle was also indicated by the reduced fluorescence from Ce6 (Figure S6, Supporting Information). When excited at 400 nm, Ce6 exhibits a characteristic emission peak at around 660 nm. However, at the same excitation wavelength, the emission from UCNP–Ce6 showed significant quenching. The reduced Ce6 fluorescence after conjugation implies that the distance between adjacent Ce6 molecules was shortened enough to induce self-quenching. The resulting UCNP–Ce6 solution was very stable in aqueous media, which was proved by measuring the hydrodynamic diameter (Figure S7, Supporting Information). The hydrodynamic diameter of UCNP–Ce6 (62.6 nm) was very similar to that of UCNPs without Ce6 conjugation (66.6 nm), suggesting that aggregation of UCNP–Ce6 was minimal upon Ce6 loading. Furthermore, UCNP–Ce6 exhibited better colloidal stability than UCNPs without Ce6 in cell culture media, probably due to enhanced hydrophobic interaction by Ce6 incorporation (Figure S8, Supporting Information). There was also no observed morphological degradation of UCNPs at pH 4.5, demonstrating that UCNPs are chemically stable in a cellular environment (Figure S9, Supporting Information).

We investigated the generation of singlet oxygen ($^1O_2$) from the UCNP–Ce6 solution. The red emission (660 nm) from UCNP–Ce6 was significantly lower than that of UCNPs owing to efficient energy transfer from UCNPs to Ce6 (Figure 1d, and Figure S10 in the Supporting Information). In contrast, the green emission was nearly unchanged after the Ce6 conjugation. Consequently, the intact green emission of UCNPs could be used for imaging, whereas the red emission could be exploited to excite Ce6 for therapeutic purposes. Generation of singlet oxygen from a UCNP–Ce6 solution was assessed using 9,10-dimethylanthracene (DMA) as a rapid chemical trap for singlet oxygen.[18] DMA is known to have a relatively high quenching rate constant and unique selectivity for singlet oxygen.[19] A UCNP–Ce6 solution was mixed with DMA and then irradiated with a 980 nm CW laser (300 mW). The fluorescence quenching of DMA during laser irradiation confirmed the generation of singlet oxygen by energy transfer from UCNPs to Ce6 (Figure 1e).

Prior to the theranostic application of UCNP–Ce6, the cytotoxicity of UCNPs with and without Ce6 was evaluated by thiazolyl blue tetrazolium bromide (MTT) assay (Figure S11, Supporting Information). Nanoparticles of various concentrations (0–0.5 mg of rare earth metal (RE) per mL) were incubated with U87MG cells for 24 h at 37 °C. Both UCNPs and UCNP–Ce6 exhibited a negligible cytotoxicity up to 0.25 mg of RE per mL, demonstrating that they are suitable for biomedical applications.

The blood circulation half-life and biodistribution of UCNPs and UCNP–Ce6 were also examined by measuring the Y^{3+} ion concentration in the blood and organs. BALB/c mice were injected with UCNPs and UCNP–Ce6 through the tail vein (0.1 mg of RE per mouse). The blood circulation half-lives of UCNPs and UCNP–Ce6 were 4.2 and 21.6 min, respectively (Figure S12, Supporting Information). The longer blood lifetime of UCNP–Ce6 may be related to the better colloidal stability of UCNP–Ce6 compared to UCNPs (Figure S8, Supporting Information). A long blood circulation time would be beneficial for imaging and diagnosis. Biodistribution of UCNPs and UCNP–Ce6 indicated that considerable numbers of UCNPs accumulated in the liver and spleen owing to the reticuloendothelial system (RES) (Figure S13, Supporting Information). The amount of UCNP–Ce6 in these organs 7 days post-injection was much lower than that of UCNPs. Facile excretion of UCNP–Ce6 would decrease the possibility of long-term toxicity.

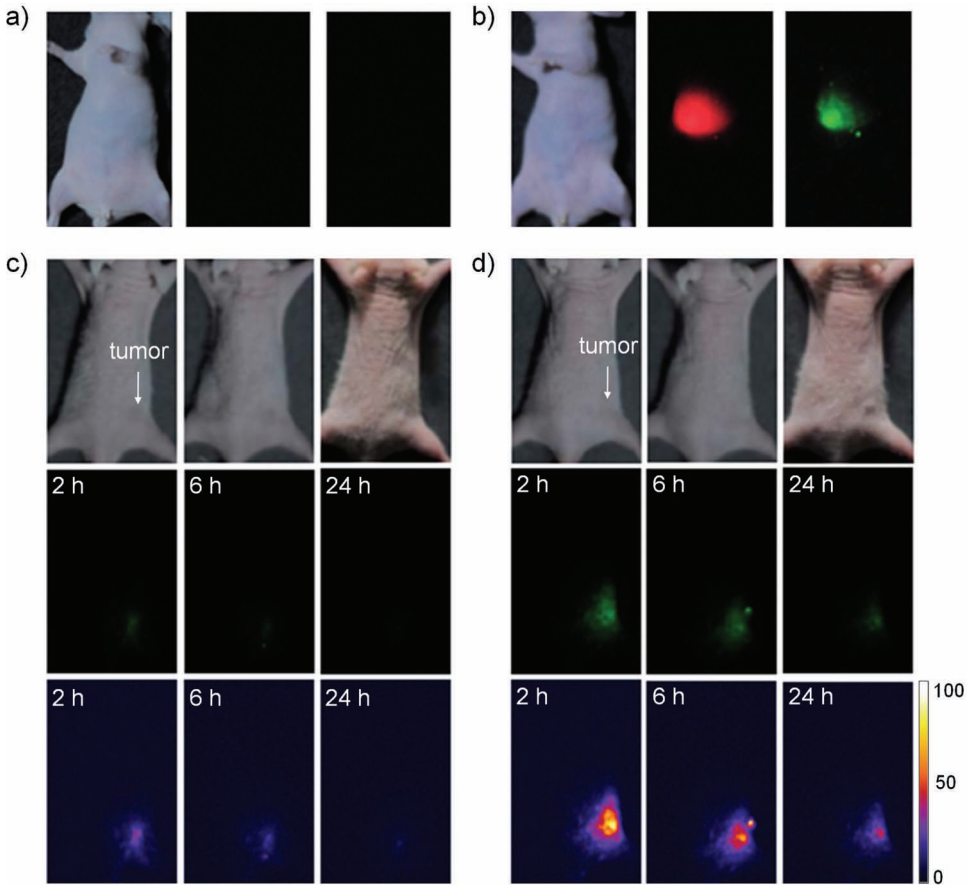

Figure 2. a,b) Upconversion luminescence images of nude mice after 1.5 h intravenous injection a) without and b) with UCNPs. Left are bright field images, middle are red luminescence images, and right are green luminescence images. c,d) Upconversion luminescence images of nude mice bearing tumor after intravenous injection of c) UCNPs and d)UCNP–Ce6. Arrows indicate tumor sites. Top row is bright field images, middle row is true-color images of green luminescence, and bottom row is pseudo-color images converted from the corresponding true-color images (middle row) using *ImageJ* image analysis software (http://rsb.info.nih.gov/ij/). Red luminescence was recorded using a red band pass filter (641.5–708.5 nm, Semrock), and green luminescence was recorded using a combination of a green band pass filter (517–567 nm, Semrock) and a 850 nm short pass filter (SPF-850, CVI).

For in vivo optical imaging studies, nude mice were injected with UCNPs through the tail vein (0.1 mg of RE per mouse) and imaged using a home-built imaging setup (Figure S14, Supporting Information). As demonstrated in the previous cellular imaging studies,[11,20] no background autofluorescence from the mouse body was observed under 980 nm irradiation without the injection of UCNPs (**Figure 2**a). Vivid green and red emissions from the liver were observed 1.5 h after the intravenous injection (Figure 2b). The red signal was more intense than the green signal, which is in accordance with the emission spectra of UCNPs in solution (Figure 1d). Because the overall hydrodynamic diameter of UCNPs coated with PEG-phospholipid was approximately 70 nm, they were rapidly accumulated in the liver and spleen, which was consistent with the biodistribution data.

In vivo tumor imaging was also performed using UCNPs. Nude mice bearing a U87MG tumor on the right hind leg were injected with UCNPs through the tail vein (0.1 mg of RE per mouse). Upconversion luminescence images of the mice were collected at different intervals, and green and red emissions from tumors were recorded (Figure 2c). The emission intensity was relatively lower than that from the liver, because the blood circulation time of UCNPs was very short, and the amount of UCNPs in the tumor tissue was much smaller than that in the liver.

Photosensitizer, Ce6, was introduced to the UCNPs not only for therapeutic effect but also for increased accumulation of UCNPs in the tumors. Owing to the lyphophilic property of Ce6, UCNP–Ce6 tends to accumulate in tumors, resulting in a significant increase in the signal-to-noise ratio.[21] Under the same measurement conditions, UCNP–Ce6 provided a clearer tumor image than UCNPs alone (Figure 2c,d). Green signals from the nanoparticles decreased with time. In the case of UCNPs, emission from the tumor was most intense 2 h after the injection, but their signal dropped rapidly, and very weak signals were detected 24 h after the injection. Unlike UCNPs, UCNP–Ce6 showed bright green signals from the tumor site for up to 6 h after the injection. Although the upconversion luminescence from UCNP–Ce6 decayed with time, the green emission persisted even 24 h after the injection; this result

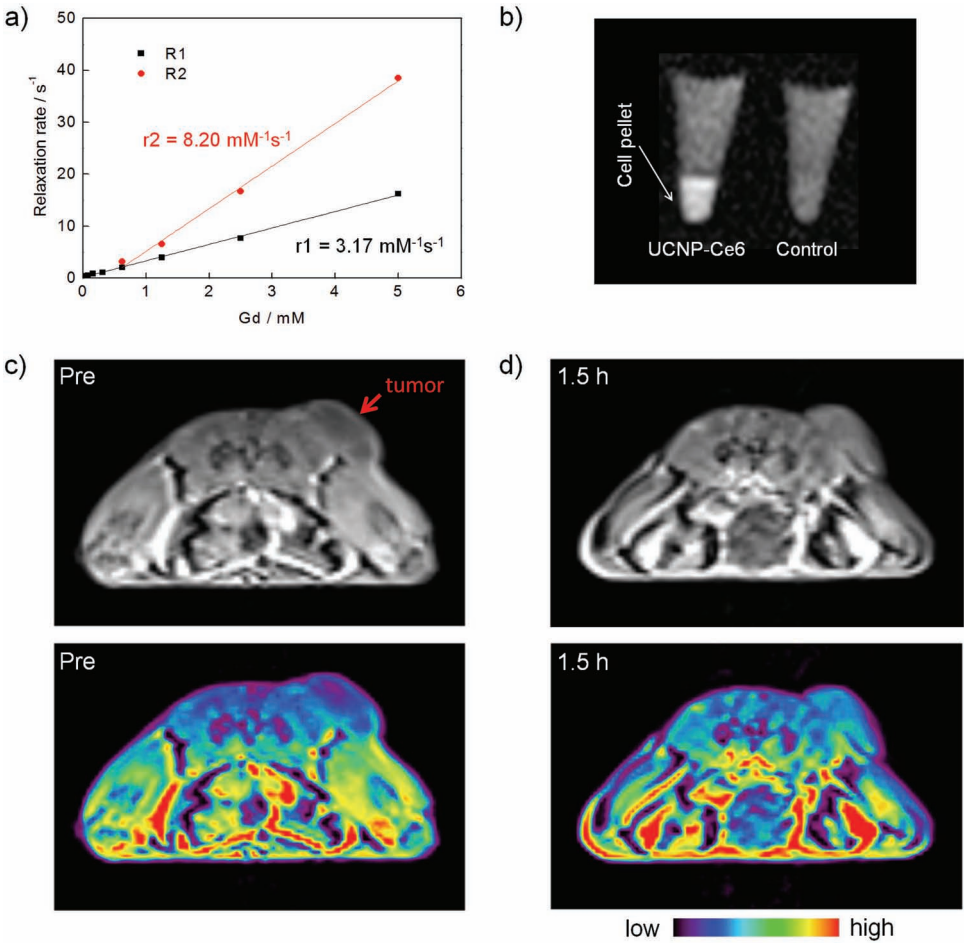

Figure 3. a) Plot of R1 (1/T1) and R2 (1/T2) as a function of Gd concentrations in water. b) T1-weighted MR images of U87MG cell pellets incubated with UCNP–Ce6 for 24 h. c,d)T1-weighted MR images (top row) and color maps of T1-weighted MR images (bottom row) of a tumor-bearing nude mouse before and after 1.5 h intravenous injection of UCNP–Ce6. Arrows indicate tumor sites. All images were recorded using a 3 T MRI scanner.

indicated that Ce6 enhanced the accumulation and retention of nanoparticles in the tumors (see also Figure S15, Supporting Information).

To demonstrate the dual-modal capability of UCNPs, T1-weighted MR images of UCNP solutions with different Gd concentrations were obtained with a 3 T clinical MRI scanner. As the concentration of Gd ions increased, the T1-weighted MR images became brighter, and the T1 relaxation time was shortened. The r1 value of the UCNPs was 3.17 mM^{-1} s^{-1} (**Figure 3**a), which is lower than that of clinically used Gd-DTPA (5–6 mM^{-1} s^{-1}). However, the r1 value was higher than that of previously reported nanoparticles of $NaGdF_4$:Yb,Er/$NaGdF_4$ (1.40 mM^{-1} s^{-1}),[11a] because Gd ions reside only at the shell matrix of the current UCNPs (Table S1, Supporting Information). Very recently, it was reported that Gd ions near the particle surface mainly contribute to the relaxivity.[22]

Along with successful luminescent tumor imaging, UCNP–Ce6 was applied to in vitro and in vivo tumor imaging by MRI. The MR contrast of U87MG cells labeled with UCNP–Ce6 (Figure 3b) was clearly enhanced, demonstrating that UCNP–Ce6 could be used as an effective T1 MRI contrast agent. For in vivo MR imaging, nude mice bearing a U87MG tumor on the right hind leg were injected with UCNP–Ce6 through the tail vein (1.5 mg of RE (0.5 mg of Gd) per mouse). Because the sensitivity of T1 MRI is considerably lower than that of luminescence imaging, in T1 MRI, 15 times more nanoparticles were injected to achieve significant contrast enhancement in tumors (Figure 3c and 3d, and Figure S16 in the Supporting Information).

Generation of singlet oxygen from UCNP–Ce6 in live cells was confirmed by using 5- (and 6-)carboxy-2′,7′-dichlorodihydrofluorescein diacetate (carboxy-H_2DCFDA) as a fluorogenic marker.[16b] In the presence of singlet oxygen, the reduced fluorescein compound is oxidized and emits bright green fluorescence. When the U87MG cells were incubated with UCNPs, the cells exhibited negligible green fluorescence under 980 nm irradiation (**Figure 4**a, and Figure S17a in the Supporting Information). However, the cells that were incubated with UCNP–Ce6 and irradiated at 980 nm showed bright green fluorescence (Figure 4b and Figure S17b in the Supporting Information). The PDT effect was also investigated by measuring cell viability using the MTT assay. There was a significant decrease in cell viability with UCNP–Ce6 and laser irradiation, whereas cell viability was nearly unchanged in the absence of laser irradiation (Figure 4c).

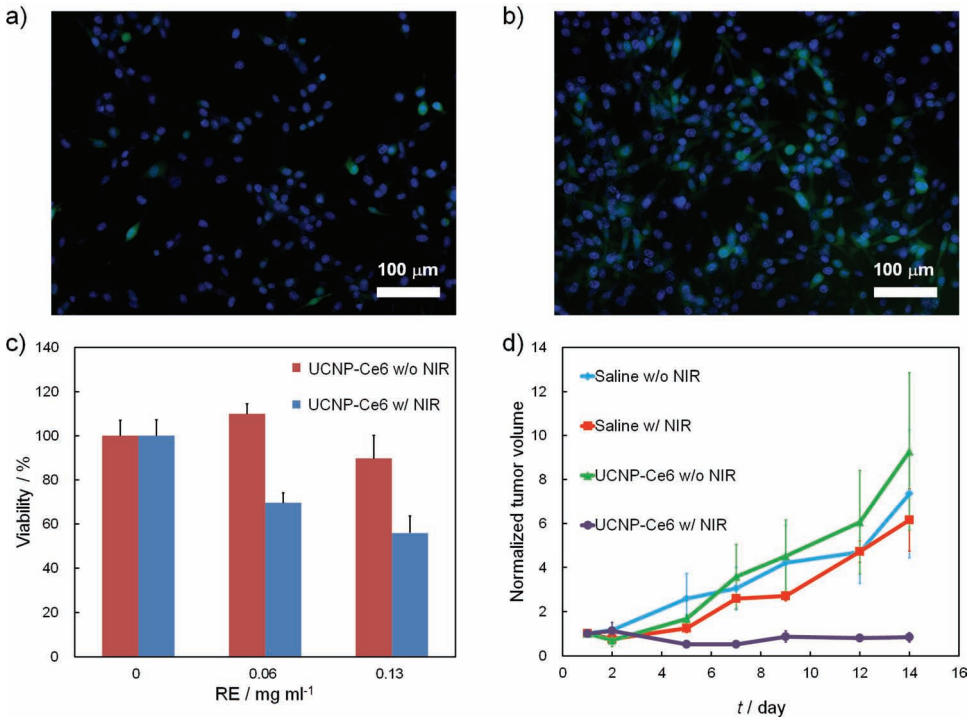

Figure 4. a,b) Detection of singlet oxygen in live cells incubated with a) UCNPs and b) UCNP-Ce6. The cells were exposed under 980 nm NIR laser (300 mW) for 5 min. Green fluorescence indicates the presence of singlet oxygen, and blue fluorescence indicates nuclei of the cells. c) Cell viability of U87MG cells incubated with UCNP–Ce6, with or without exposure to 980 nm laser ($n = 5$ for each group). d) Growth of tumors after treatments ($n = 3$ for each group). The relative tumor volumes were normalized to their initial sizes.[16d,23]

In vivo PDT was also performed using UCNP–Ce6 (Figure 4d). Nude mice bearing a U87MG tumor on the right hind leg were injected with UCNP–Ce6 through the tail vein (0.1 mg of RE per mouse). Under 980 nm irradiation, tumor growth was inhibited, while non-treated tumors grew significantly. Histological examination also confirmed the tumor necrosis induced by UCNP–Ce6 and laser irradiation (Figure S18, Supporting Information). These results clearly demonstrate the clinical applicability of UCNP–Ce6 as PDT agents.

In summary, dual-modal in vivo tumor imaging and PDT were performed using photosensitizer-conjugated lanthanide-doped nanoparticles. Hexagonal phase $NaYF_4$:Yb,Er/$NaGdF_4$ core–shell UCNPs could be used for both in vivo luminescence imaging and MRI and conjugated with Ce6, a PDT drug. UCNP–Ce6 nanoparticles were readily accumulated in tumor sites by the EPR effect. Tumors could be clearly observed not only in the upconversion luminescence image but also in the MR image. Upon irradiation by a 980 nm laser, UCNPs could transfer the excitation energy to Ce6, which could then generate cytotoxic singlet oxygen. Through the systemic administration of UCNP–Ce6 followed by 980 nm irradiation, an in vivo PDT effect could be demonstrated. These results clearly indicate that UCNP–Ce6 can be used not only as dual-modal imaging probes for accurate diagnosis but also as PDT agents for efficient therapy.

Supporting Information

Supporting Information is available from the Wiley Online Library or from the author.

Acknowledgements

T.H. acknowledges the financial support by the National Research Foundation (NRF) of Korea through Strategic Research (2010-0029138), Global Research Laboratory (2011-0021628), and World Class University (R31-10013) Programs. S.H.L. was supported by a Korea University Grant. Y.S.Y. acknowledges the financial support by the Industrial Core Technology Development Program (10037397) of MKE and Basic Science Research Program (R11-2008-044-03004-0) of NRF. Y.D.S. was supported by KRICT (SI-1110), the Nano R&D Program (2011-0019156) of NRF, the Industrial Core Technology Development Program (10037397) of MKE, and the Development of Advanced Scientific Analysis Instrumentation Project of KRISS by MEST. K.T.L. was supported by the Nano R&D Program (2010-0019142), the Pioneer Research Center Program (2010-0002195) of NRF, and the Industrial Core Technology Development Program (10033183) of MKE. H.M.K. was supported by the Public Welfare & Safety Research Program (2011-0020957) of NRF. Y.I.P., H.M.K., and J.H.K. contributed equally to this work.

Received: June 15, 2012
Published online: August 23, 2012

[1] a) B. Dubertret, P. Skourides, D. J. Norris, V. Noireaux, A. H. Brivanlou, A. Libchaber, *Science* **2002**, *298*, 1759; b) S. Kim, Y. T. Lim, E. G. Soltesz, A. M. De Grand, J. Lee, A. Nakayama, J. A. Parker, T. Mihaljevic, R. G. Laurence, D. M. Dor, L. H. Cohn, M. G. Bawendi, J. V. Frangioni, *Nat. Biotechnol.* **2004**, *22*, 93; c) X. Gao, Y. Cui, R. M. Levenson, L. W. K. Chung, S. Nie, *Nat. Biotechnol.* **2004**, *22*, 969; d) X. Michalet, F. F. Pinaud, L. A. Bentolila, J. M. Tsay, S. Doose, J. J. Li, G. Sundaresan, A. M. Wu, S. S. Gambhir, S. Weiss, *Science* **2005**, *307*, 538; e) J. Rao, A. Dragulescu-Andrasi, H. Yao, *Curr. Opin. Biotechnol.* **2007**, *18*, 17.

[2] a) M. G. Harisinghani, J. Barentsz, P. F. Hahn, W. M. Deserno, S. Tabatabaei, C. H. van de Kaa, J. de la Rosette, R. Weissleder, *New Engl. J. Med.* **2003**, *348*, 2491; b) J. W. M. Bulte, D. L. Kraitchman, *NMR Biomed.* **2004**, *17*, 484; c) Y.-M. Huh, Y.-w. Jun, H.-T. Song, S. Kim, J.-s. Choi, J.-H. Lee, S. Yoon, K.-S. Kim, J.-S. Shin, J.-S. Suh, J. Cheon, *J. Am. Chem. Soc.* **2005**, *127*, 12387; d) H. B. Na, I. C. Song, T. Hyeon, *Adv. Mater.* **2009**, *21*, 2133; e) N. Lee, T. Hyeon, *Chem. Soc. Rev.* **2012**, *41*, 2575.

[3] a) J. Cheon, J.-H. Lee, *Acc. Chem. Res.* **2008**, *41*, 1630; b) L. E. Jennings, N. J. Long, *Chem. Commun.* **2009**, 3511; c) J. Kim, Y. Piao, T. Hyeon, *Chem. Soc. Rev.* **2009**, *38*, 372; d) C. Tassa, S. Y. Shaw, R. Weissleder, *Acc. Chem. Res.* **2011**, *44*, 842.

[4] a) L. Prinzen, R.-J. J. H. M. Miserus, A. Dirksen, T. M. Hackeng, N. Deckers, N. J. Bitsch, R. T. A. Megens, K. Douma, J. W. Heemskerk, M. E. Kooi, P. M. Frederik, D. W. Slaaf, M. A. M. J. van Zandvoort, C. P. M. Reutelingsperger, *Nano Lett.* **2007**, *7*, 93; b) H. Lee, M. K. Yu, S. Park, S. Moon, J. J. Min, Y. Y. Jeong, H.-W. Kang, S. Jon, *J. Am. Chem. Soc.* **2007**, *129*, 12739; c) J.-L. Bridot, A.-C. Faure, S. Laurent, C. Rivière, C. Billotey, B. Hiba, M. Janier, V. Josserand, J.-L. Coll, L. Vander Elst, R. Muller, S. Roux, P. Perriat, O. Tillement, *J. Am. Chem. Soc.* **2007**, *129*, 5076; d) Y.-s. Yoon, B.-I. Lee, K. S. Lee, G. H. Im, S.-H. Byeon, J. H. Lee, I. S. Lee, *Adv. Funct. Mater.* **2009**, *19*, 3375; e) A. Gianella, P. A. Jarzyna, V. Mani, S. Ramachandran, C. Calcagno, J. Tang, B. Kann, W. J. R. Dijk, V. L. Thijssen, A. W. Griffioen, G. Storm, Z. A. Fayad, W. J. M. Mulder, *ACS Nano* **2011**, *5*, 4422.

[5] a) D. R. Gamelin, H. U. Güdel, *Acc. Chem. Res.* **2000**, *33*, 235; b) F. Wang, R. Deng, J. Wang, Q. Wang, Y. Han, H. Zhu, X. Chen, X. Liu, *Nat. Mater.* **2011**, *10*, 968.

[6] a) F. Auzel, *Chem. Rev.* **2004**, *104*, 139; b) J. F. Suyver, A. Aebischer, D. Biner, P. Gerner, J. Grimm, S. Heer, K. W. Krämer, C. Reinhard, H. U. Güdel, *Opt. Mater.* **2005**, *27*, 1111; c) F. Wang, X. Liu, *Chem. Soc. Rev.* **2009**, *38*, 976; d) M. Haase, H. Schäfer, *Angew. Chem. Int. Ed.* **2011**, *50*, 5808.

[7] P. Pantazis, J. Maloney, D. Wu, S. E. Fraser, *Proc. Natl. Acad. Sci. USA* **2010**, *107*, 14535.

[8] a) M. Albota, D. Beljonne, J.-L. Brédas, J. E. Ehrlich, J.-Y. Fu, A. A. Heikal, S. E. Hess, T. Kogej, M. D. Levin, S. R. Marder, D. McCord-Maughon, J. W. Perry, H. Röckel, M. Rumi, G. Subramaniam, W. W. Webb, X.-L. Wu, C. Xu, *Science* **1998**, *281*, 1653; b) D. R. Larson, W. R. Zipfel, R. M. Williams, S. W. Clark, M. P. Bruchez, F. W. Wise, W. W. Webb, *Science* **2003**, *300*, 1434.

[9] a) S. Heer, K. Kömpe, H.-U. Güdel, M. Haase, *Adv. Mater.* **2004**, *16*, 2102; b) J.-C. Boyer, L. A. Cuccia, J. A. Capobianco, *Nano Lett.* **2007**, *7*, 847; c) Z. Li, Y. Zhang, *Nanotechnology* **2008**, *19*, 345606; d) F. Wang, Y. Han, C. S. Lim, Y. Lu, J. Wang, J. Xu, H. Chen, C. Zhang, M. Hong, X. Liu, *Nature* **2010**, *463*, 1061; e) X. Ye, J. E. Collins, Y. Kang, J. Chen, D. T. N. Chen, A. G. Yodh, C. B. Murray, *Proc. Natl. Acad. Sci. USA* **2010**, *107*, 22430; f) F. Wang, J. Wang, X. Liu, *Angew. Chem. Int. Ed.* **2010**, *49*, 7456; g) L. Cheng, K. Yang, Y. Li, J. Chen, C. Wang, M. Shao, S.-T. Lee, Z. Liu, *Angew. Chem. Int. Ed.* **2011**, *50*, 7385; h) R. Deng, X. Xie, M. Vendrell, Y.-T. Chang, X. Liu, *J. Am. Chem. Soc.* **2011**, *133*, 20168.

[10] C. T. Xu, N. Svensson, J. Axelsson, P. Svenmarker, G. Somesfalean, G. Chen, H. Liang, H. Liu, Z. Zhang, S. Andersson-Engels, *Appl. Phys. Lett.* **2008**, *93*, 171103.

[11] a) Y. I. Park, J. H. Kim, K. T. Lee, K.-S. Jeon, H. B. Na, J. H. Yu, H. M. Kim, N. Lee, S. H. Choi, S.-I. Baik, H. Kim, S. P. Park, B.-J. Park, Y. W. Kim, S. H. Lee, S.-Y. Yoon, I. C. Song, W. K. Moon, Y. D. Suh, T. Hyeon, *Adv. Mater.* **2009**, *21*, 4467; b) S. Wu, G. Han, D. J. Milliron, S. Aloni, V. Altoe, D. V. Talapin, B. E. Cohen, P. J. Schuck, *Proc. Natl. Acad. Sci. USA* **2009**, *106*, 10917.

[12] R. A. Jalil, Y. Zhang, *Biomaterials* **2008**, *29*, 4122.

[13] a) R. Kumar, M. Nyk, T. Y. Ohulchanskyy, C. A. Flask, P. N. Prasad, *Adv. Funct. Mater.* **2009**, *19*, 853; b) Z. Li, Y. Zhang, B. Shuter, N. M. Idris, *Langmuir* **2009**, *25*, 12015.

[14] a) J. Zhou, Y. Sun, X. Du, L. Xiong, H. Hu, F. Li, *Biomaterials* **2010**, *31*, 3287; b) J. Zhou, M. Yu, Y. Sun, X. Zhang, X. Zhu, Z. Wu, D. Wu, F. Li, *Biomaterials* **2011**, *32*, 1148; c) H. Xing, W. Bu, S. Zhang, X. Zheng, M. Li, F. Chen, Q. He, L. Zhou, W. Peng, Y. Hua, J. Shi, *Biomaterials* **2012**, *33*, 1079.

[15] a) J. D. Bhawalkar, N. D. Kumar, C.-F. Zhao, P. N. Prasad, *J. Clin. Laser Med. Surg.* **1997**, *15*, 201; b) D. E. J. G. J. Dolmans, D. Fukumura, R. K. Jain, *Nat. Rev. Cancer* **2003**, *3*, 380; c) H. Gu, K. Xu, Z. Yang, C. K. Chang, B. Xu, *Chem. Commun.* **2005**, 4270; d) Y. Cheng, A. C. Samia, J. D. Meyers, I. Panagopoulos, B. Fei, C. Burda, *J. Am. Chem. Soc.* **2008**, *130*, 10643.

[16] a) B. Ungun, R. K. Prud'homme, S. J. Budijono, J. Shan, S. F. Lim, Y. Ju, R. Austin, *Opt. Express* **2009**, *17*, 80; b) H. Guo, H. Qian, N. M. Idris, Y. Zhang, *Nanomed.: Nanotechnol. Biol. Med.* **2010**, *6*, 486; c) J. Shan, S. J. Budijono, G. Hu, N. Yao, Y. Kang, Y. Ju, R. K. Prud'homme, *Adv. Funct. Mater.* **2011**, *21*, 2488; d) C. Wang, H. Tao, L. Cheng, Z. Liu, *Biomaterials* **2011**, *32*, 6145.

[17] a) K. A. Abel, J.-C. Boyer, F. C. J. M. van Veggel, *J. Am. Chem. Soc.* **2009**, *131*, 14644; b) K. A. Abel, J.-C. Boyer, C. M. Andrei, F. C. J. M. van Veggel, *J. Phys. Chem. Lett.* **2011**, *2*, 185.

[18] B.-c. Bae, K. Na, *Biomaterials* **2010**, *31*, 6325.

[19] K. Tanaka, T. Miura, N. Umezawa, Y. Urano, K. Kikuchi, T. Higuchi, T. Nagano, *J. Am. Chem. Soc.* **2001**, *123*, 2530.

[20] a) M. Nyk, R. Kumar, T. Y. Ohulchanskyy, E. J. Bergey, P. N. Prasad, *Nano Lett.* **2008**, *8*, 3834; b) F. Vetrone, R. Naccache, A. J. de la Fuente, F. Sanz-Rodríguez, A. Blazquez-Castro, E. M. Rodriguez, D. Jaque, J. G. Solé, J. A. Capobianco, *Nanoscale* **2010**, *2*, 495; c) S. H. Nam, Y. M. Bae, Y. I. Park, J. H. Kim, H. M. Kim, J. S. Choi, K. T. Lee, T. Hyeon, Y. D. Suh, *Angew. Chem. Int. Ed.* **2011**, *50*, 6093.

[21] S. Y. Park, H. J. Baik, Y. T. Oh, K. T. Oh, Y. S. Youn, E. S. Lee, *Angew. Chem. Int. Ed.* **2011**, *50*, 1644.

[22] a) F. Chen, W. Bu, S. Zhang, X. Liu, J. Liu, H. Xing, Q. Xiao, L. Zhou, W. Peng, L. Wang, J. Shi, *Adv. Funct. Mater.* **2011**, *21*, 4285; b) N. J. J. Johnson, W. Oakden, G. J. Stanisz, R. S. Prosser, F. C. J. M. van Veggel, *Chem. Mater.* **2011**, *23*, 3714.

[23] J.-H. Lee, J.-t. Jang, J.-s. Choi, S. H. Moon, S.-h. Noh, J.-w. Kim, J.-G. Kim, I.-S. Kim, K. I. Park, J. Cheon, *Nat. Nanotechnol.* **2011**, *6*, 418.